Assembly and Test of a Support Structure for 3.6 m Long Nb_3Sn Racetrack Coils

P. Ferracin, G. Ambrosio, M. Anerella, S. Caspi, D. W. Cheng, H. Felice, A. R. Hafalia, C. R. Hannaford, A. F. Lietzke, J. Lizarazo, J. Muratore, G. L. Sabbi, J. Schmalzle, R. Thomas, and P. J. Wanderer

***Abstract*— The LHC Accelerator Research Program (LARP) is currently developing 4 m long Nb_3Sn quadrupole magnets for a possible upgrade of the LHC Interaction Regions (IR). In order to provide a reliable test bed for the fabrication and test of long Nb_3Sn coils, LARP has started the development of the long racetrack magnet LRS01. The magnet is composed of two 3.6 m long racetrack coils contained in a support structure based on an aluminum shell pre-tensioned with water-pressurized bladders and interference keys. For the phase-one test of the assembly procedure and loading operation, the structure was pre-stressed at room temperature and cooled down to 77 K with instrumented, solid aluminum "dummy coils". Mechanical behavior and stress homogeneity were monitored with strain gauges mounted on the shell and the dummy coils. The dummy coils were replaced with reacted and impregnated Nb_3Sn coils in a second assembly procedure, followed by cool-down to 4.5 K and powered magnet test. This paper report on the assembly and loading procedures of the support structure as well as the comparison between strain gauge data and 3D model predictions.**

***Index Terms*— LARP, superconducting magnets, Nb_3Sn**

I. INTRODUCTION

THE long racetrack (LR) magnet series [1]-[2] is under development by the U.S. LHC Accelerator Research Program (LARP) [3] to demonstrate that 1) Nb_3Sn superconducting coils can be fabricated in lengths significantly longer than one meter, and 2) supporting structures based on an aluminum shell pre-tensioned with water-pressurized bladders can be scaled up for long accelerator magnets. The first magnet of the series, LRS01, was recently tested at Brookhaven National Laboratory (BNL) [4]. We report in this paper the development and test of the LR support structure, and the analysis of strain gauge data and finite element results.

Manuscript received August 28, 2007. This work was supported by the Director, Office of Energy Research, Office of High Energy and Nuclear Physics, High Energy Physics Division, U. S. Department of Energy, under Contract No. DE-AC02-05CH11231.

P. Ferracin, S. Caspi , D.W. Cheng, A. R. Hafalia, C.R. Hannaford, A. F. Lietzke, J. Lizarazo and G. L. Sabbi are with Lawrence Berkeley National Lab, Berkeley, CA 94720, USA (phone: 510-486-4630; fax: 510-486-5310; e-mail: pferracin@lbl.gov).

G. Ambrosio, is with Fermi National Accelerator Laboratory, Batavia, IL 60510, USA.

M. Anerella, J. Muratore, J. Schmalzle, R. Thomas and P. Wanderer are with Brookhaven National Laboratory, Upton, NY 11973-5000, USA.

II. MAGNET DESIGN

The LR magnet design is based on the Subscale Magnet (SM) series developed at Lawrence Berkeley National Laboratory (LBNL) [5]. It consists of two 3.6 meter long racetrack Nb_3Sn coils connected in a common-coil configuration [6]. The cross-section and the end region design are depicted in Fig. 1.

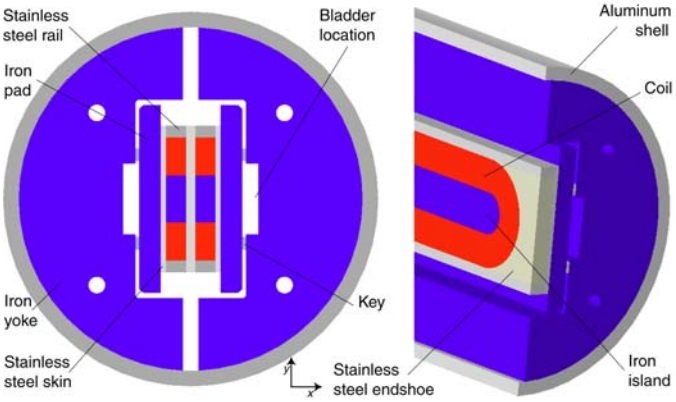

Fig. 1. LRS01 cross-section (left) and end design (right).

Each of the two coil modules is composed of two layers (21 turns each) wound around an iron island and constrained in the ends by two stainless steel end shoe. The entire length, including the straight section, is constrained by 3.6 m long stainless steel rails and skins. Two iron pad sub-assemblies, each consisting of two 1.8 m long machines plates, are bolted-up around the two coil modules and provide initial pre-stress. This "coil-pack" sub-assembly is then inserted into a structure composed by a 3.6 m long aluminum shell and 50 mm thick iron yoke laminations. The laminations include machined grooves to provide room for 4 water-pressurized bladders, each 1.8 m long, inserted from each end.

TABLE I MAGNET PARAMETERS

	Unit	
B_{peak}(4.5 K)	T	12.0
I_{ss} (4.5 K)	kA	10.6
F_x per quadrant @ I_{ss}	kN/m	+ 1835
F_y per quadrant @ I_{ss}	kN/m	- 12
F_z per quadrant @ I_{ss}	kN	19

The bladder pressurization stretches the shell and compresses the coil-pack, and allows the insertion of four iron

interference keys and shims. Once the bladders are deflated and removed, the aluminum shell collapses on the keys and pre-loads the coil-pack. Additional pre-load is provided by the shell to the coil during cool-down, because of the higher thermal contraction of aluminum with respect to the other materials. The magnet parameters are given in Table I: the expected maximum current at 4.5 K based on extracted strand measurements is 10.6 kA, with a coil peak field of 12.0 T.

III. Instrumentation

The shell was instrumented with half-bridge strain gauges placed on the right side and left side of the magnet mid-plane (see Fig. 2). The gauges measure the azimuthal and axial strain at six longitudinal stations along the shell: station 1 is near the lead end and station 5 is at the shell's longitudinal center. In total, 24 gauges, all thermally compensated by gauges mounted on stress-free aluminum elements, were mounted on the shell. The gauges in stations 1 and 2 (end gauges) were used to monitor end effects, whereas the ones in stations 3 to 6 (central gauges) measured strain variations in the central part of the magnet. The measured strain in the azimuthal and axial directions (ε_θ and ε_z) was converted into stress (σ_θ and σ_z) using the relation

$$\sigma_{\theta,z} = \frac{E}{\left(1-\nu^2\right)}\left(\varepsilon_{\theta,z} + \nu\varepsilon_{z,\theta}\right), \qquad (1)$$

where E and ν are, respectively, the elastic modulus (79 GPa at 4.5 K) and the Poisson's ratio (0.34) of aluminum.

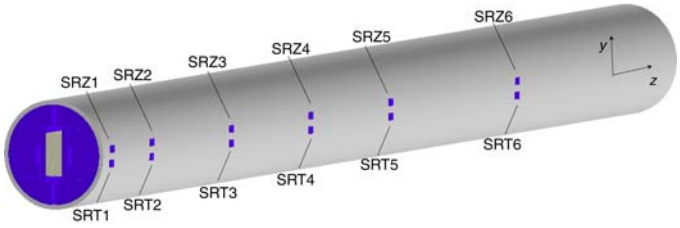

Fig. 2. Location of azimuthal (T) and axial (Z) shell gauges on the shell right side (R). The same gauge configuration is mounted on the left side (L).

IV. Assembly

The assembly of the LR support structure required the use of several specially designed fixtures (see Fig 3): two identical steel "rafts", each with five equally-spaced aluminum cradles, and two steel installation beams with machined keyways matching the interference key slots of the yokes and the pads. The first beam ("insertion beam") is where the yoke laminations and the coil-pack are assembled before being slid onto the shell. The second beam ("cantilevered beam") is attached to the end of the insertion beam and positioned inside the shell. The cantilevered beam features five removable aluminum supports, which rest on the internal shell surface and five hydraulic pistons, mounted inside the beam itself. Both the removable supports and the pistons are positioned at the same locations as the external shell cradles on the rafts.

The assembly and loading procedures, performed with the structure rotated 90° with respect to the cross-section shown in Fig. 1 (left), proceeded as follows: the instrumented shell was first placed on one support raft, which was leveled and aligned on a granite precision surface plate. The cantilevered beam was then inserted into the shell, and connected and aligned with the insertion beam, pre-assembled on the second raft resting on a second precision surface plate. At this point, the stack of yoke half-laminations was assembled on the installation beam and tied together with two 12.7 mm diameter tie-rods. Using a cable winch mounted at the opposite end of the cantilever beam, the yoke stack was then pulled into the shell on brass keys positioned in the beams' keyways. With the first stack of yoke laminations resting inside the shell on the cantilevered beam, the installation beam assembly was disconnected and removed from its support raft. This second raft was placed over the shell and bolted to the shell's support raft at the cradles, thus clamping the shell assembly into a unitized structure. Then the hydraulic pistons were pressurized and locked to press the yoke stack assembly into firm contact with the upper surface of the shell.

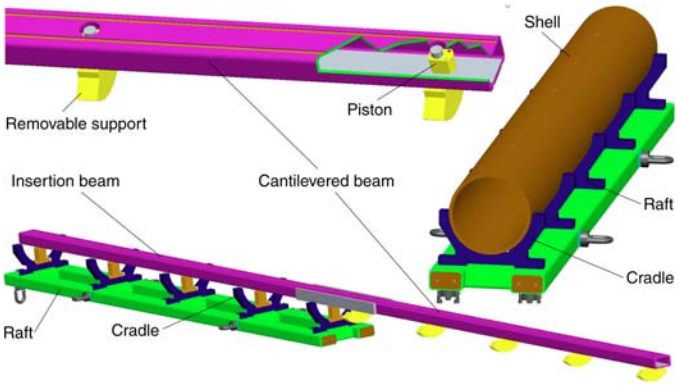

Fig. 3. Assembly tools: beams, cradles and rafts.

Large aluminum discs were then mounted at both ends of the yoke, shell, and raft assembly, and, with the pistons still pressurized and locked, the entire assembly was lifted by a crane onto the floor and rolled 180° (see Fig. 4). After placing the structure back on the granite table, with the yoke laminations now resting on the bottom surface of the shell, the aluminum discs were unbolted from the rafts, and the piston pressure was released. The upper raft was then removed from the assembly, repositioned at the end of the shell, and realigned a second time with the installation beam. At the same time, the cantilever beam was pulled out and, after the removal of the aluminum supports, re-inserted inside the shell on top of the first yoke half.

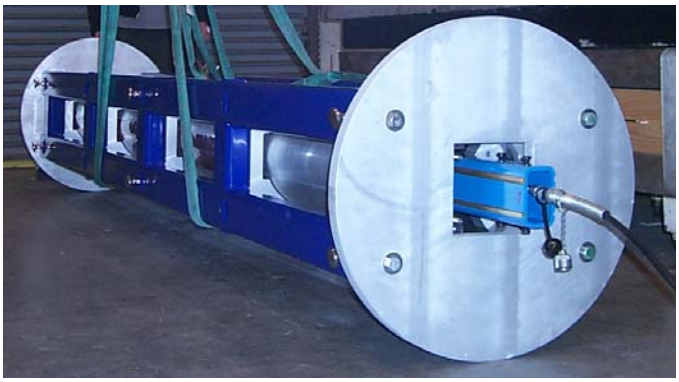

Fig. 4. Rotation of the support structure.

The process of assembling the second stack of yoke laminations and pulling it into the shell structure was then

repeated. Once inserted, the second yoke half was pressed into firm contact with the shell by actuating the pistons of the cantilevered beam, and yoke gap keys were inserted in the gap between the yoke halves. After the release of the piston, the gap keys locked the iron laminations in position with a minimal pre-tension in the shell and the cantilever beam was pulled out from the structure. In parallel, the dummy coil-pack, composed of the load pads and the two aluminum dummy coils, was assembled and placed on the insertion beam. The assembled coil stack was then pulled into the structure sliding on shimmed keys, whose thickness was chosen to place the coil in the theoretical center of the assembly after loading. At this point, the assembly was ready for pre-loading operation with the bladders.

V. Loading, Cool-down, and Excitation

A. Design expectations

The mechanical behavior and the stress targets for LRS01 were analyzed by an ANSYS 3D finite element model of the entire magnet geometry. The code computed the stress on coil and structure from 293 K to short sample field. Based on experimental data from the LBNL Subscale Model Program [5], a target shell azimuthal stress of 200 ± 50 MPa at 4.5 K was chosen. Along the axial direction, the model predicted a relative displacement of the shell with respect of the yoke, strongly dependent on the friction factor assumed between the aluminum cylinder and the iron laminations. The shell-yoke interaction is shown in Fig. 5, where the computed relative displacement between the two components at 4.5 K versus the axial location z (z = 0 at the magnet center) is plotted assuming different friction factors. In the graph, a negative displacement corresponds to a relative displacement of the shell towards the center of the magnet. In frictionless conditions, during cool-down, the shell contracts freely along the z direction and slides on the iron yoke because of 1) the higher thermal contraction of aluminum and 2) the Poisson's effect related to the increase in azimuthal strain ($-\nu\varepsilon_\theta$). As a result, the model predicts that the shell which at 4.5 K is about 5.3 mm shorter than the yoke (per half magnet length). When friction is included, the shell's contraction is partially limited and the relative displacement in the ends is reduced to 2.7 mm and 1.4 mm, respectively with a 0.1 and 0.2 friction factor.

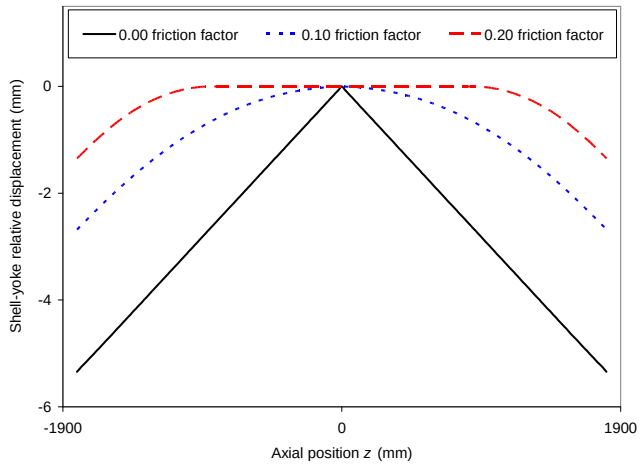

Fig. 5. Computed relative displacement (mm) between shell and yoke at 4.5 K with different friction factors, as a function of the shell axial position (mm).

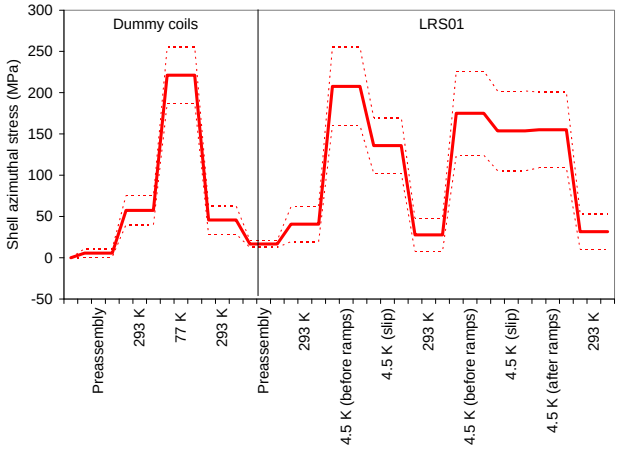

Fig. 6. Measured azimuthal shell stress during loading with dummy coils and during the LRS01 test: average of the central gauges (solid line) with ± 1 × rms (dashed line).

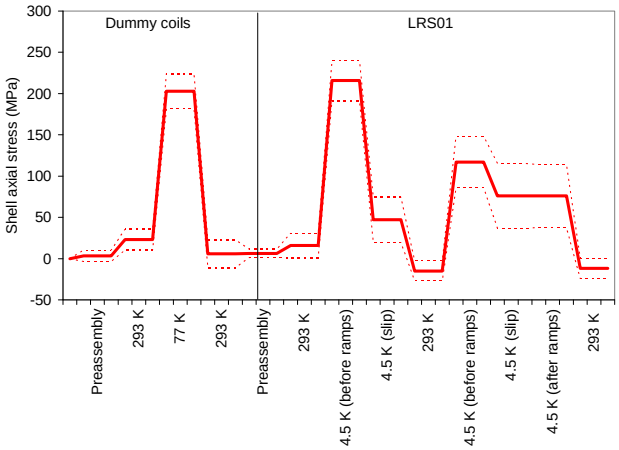

Fig. 7. Measured axial shell stress during loading with dummy coils and during the LRS01 test: average of the central gauges (solid line) with ± 1 × rms (dashed line).

In addition, a central zone with no relative displacement appears in the central section of the shell: with a 0.2 friction factor, the shell slides on the yoke only over about 1 m of length starting from the ends, while a central section of approximately 1.8 m in length remains locked to the yoke.

B. Measurements

The evolution of the shell stress from the initial loading with dummy coils to the final test of LRS01 is given in Fig. 6 and Fig 7. After pulling the dummy coil-pack into the shell-yoke sub-assembly, two 1.8 m long bladders were inserted from both magnet ends in the slot between the upper pad and the upper yoke. The bladders were pressurized up to 50 MPa to allow the insertion of the upper interference keys. After the bladders were deflated, the azimuthal shell stress measured by the central gauges was 57 ± 18 MPa (1 × rms). The structure was then clamped in between the two rafts (see Fig. 8), crated, and shipped to BNL, for the cool-down test at 77 K. After cool-down, the azimuthal stress in the central part of the shell increased to 221 ± 34 MPa. At the same time, in the axial direction, the contact friction with the iron laminations prevented the aluminum shell from shrinking longitudinally. As a result, the shell reached an axial tension of 203 ± 21 MPa. Once the structure was brought to room temperature, the bladder operation was repeated to unload and remove the

dummy coil-pack, and the loading procedures were repeated a second time with the LRS01 Nb_3Sn coils. During the cool-down to 4.5 K, the shell reached similar stress values as in the first cool-down to 77 K, both in the azimuthal (208 ± 47 MPa) and axial (216 ± 21 MPa) direction.

Fig. 8. LRS01 support structure after assembly of the dummy coil-pack. The shell is clamped by aluminum cradles connected to steel beams.

However, when the magnet was ramped to 6000 A for the first scheduled quench-heater test, the shell suddenly slipped axially with respect to the yoke. This was evidenced in the data by a sudden drop in axial tension to 47 ± 27 MPa. As a consequence, the azimuthal stress decreased by about 70 MPa. The slippage did not induce any quench in the coil, but the test was interrupted because of an unrelated contamination in the cryogenic system. After warm-up, the shell remained in partial compression along the axial direction, indicating that the friction with the yoke was now limiting the shell thermal expansion. After the third and last cool-down, the shell experienced a second slippage at 3000 A, after which the stress remained stable during test at about 155 ± 46 and 67 ± 39 MPa in the azimuthal and axial direction respectively. The training started above 80% of the magnet short sample current (I_{ss}), and after 5 quenches, it reached a plateau at 91% of I_{ss}.

VI. Strain Variations Along Axial Direction

A. Axial Strain

In Fig. 9, the measurements of the axial strain are plotted as a function of the axial position. After the first cool-down of LRS01, the measured axial strain increased from about -100 microstrain in the end region to a maximum of + 2000 microstrain in the center, in agreement with model results (assuming a friction factor of 0.2 between shell and yoke).

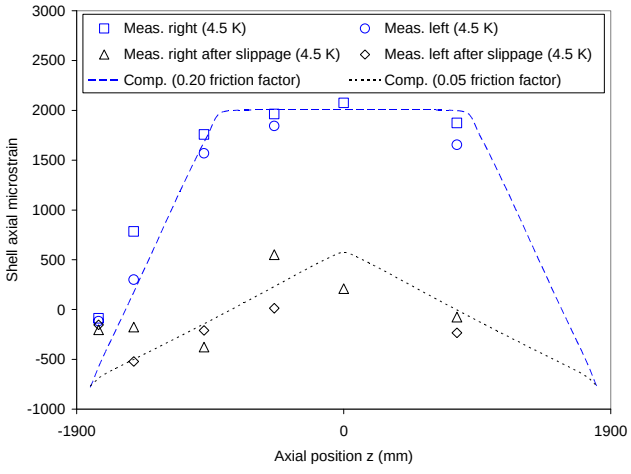

Fig. 9. Axial shell strain as a function of axial position after first cool-down and the first slippage of LRS01: measured data (markers), and computation results with different friction factors (dashed lines).

Regarding the sudden slippages that took place during excitation, a possible cause could be related to the mechanical effect of the e.m. forces, which, by deforming the yoke, may alter the contact surface between yoke and shell. As a consequence, it is possible that from a condition of 0.2 "static friction" factor, the shell-yoke interface moves to a 0.05 "dynamic friction" factor (see Fig. 8). Results from the 3D model indicate that the issue of the slippage could be addressed by segmenting the shell in four parts, thus reducing the maximum shell axial strain from 2000 to 500 microstrain.

B. Azimuthal strain

In Fig. 10 the azimuthal strain at 293 K and 4.5 K measured during the first cool-down of LRS01is plotted. Significant left-right asymmetries and variation along the shell are observed. Consistently with data, numerical computations estimate that the range of azimuthal strain variation due to fabrication tolerances of shell and yoke (± 30 μm for the shell inner radius and ± 40 μm for the yoke outer radius) is of ± 350 microstrain.

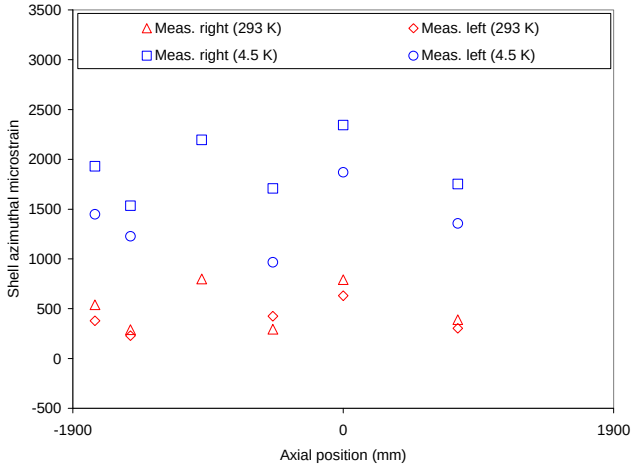

Fig. 10. Measured azimuthal shell strain as a function of axial position before and after the first cool-down of LRS01.

VII. Conclusions

The first shell-based long structure has been successfully assembled, pre-loaded with pressurized bladders, and cooled down for the test of LRS01, a 3.6 m long racetrack magnet. High axial tension, with sudden slippages over the course of the test, and variations in azimuthal strain were recorded by gauges mounted on the shell. As a possible solution, segmented shell with tighter tolerances is being considered to improve strain uniformity.

References

[1] P. Wanderer, *et al.*, "LARP Long Nb_3Sn Racetrack Coil Program", *IEEE Trans. Appl. Supercond.*, vol. 17, no. 2, June 2007, pp. 1140-1143.

[2] G. Ambrosio, *et al.*, "Design of Nb_3Sn Coils for LARP Long Magnets", *IEEE Trans. Appl. Supercond.*, vol. 17, no. 2, June 2007, pp. 1035-1038.

[3] S.A. Gourlay, *et al.*, "Magnet R&D for the IS LHC Accelerator Research Program", *IEEE Trans. Appl. Supercond.*, vol. 16, no. 2, June 2006, pp. 324-327.

[4] P.J. Wanderer, *et al.*, "Construction and Test of 4m Nb3Sn Racetrack Coils for LARP", presented at *20th International Conference on Magnet Technology*, Philadelphia, PA, USA, August 27-31, 2007.

[5] A. R. Hafalia, *et al.*, "An approach for faster high field magnet technology development", *IEEE Trans. Appl. Supercond.*, vol. 13, no. 2, June 2003, pp. 1258-1261.

[6] P. Ferracin, *et al.*, "Design and fabrication of a supporting structure for 3.6 m Long Nb_3Sn racetrack coils", *IEEE Trans. Appl. Supercond.*, vol. 17, no. 2, June 2007, pp. 1023-1026.